


# Homoclinic chaos in strongly dissipative strongly coupled complex dusty plasmas

Samiran Ghosh

*Department of Applied Mathematics, University of Calcutta, 92 Acharya Prafulla Chandra Road, Kolkata-700 009, India*

 (Received 27 July 2020; revised 19 December 2020; accepted 22 January 2021; published 9 February 2021)

The transport properties of the weakly nonlinear (WNL) two-dimensional (2D) quasilongitudinal dust lattice mode is studied in an experimentally realized highly viscous, strongly coupled, weakly ionized plasma [V. E. Fortov *et al.*, *Phys. Rev. Lett.* **109**, 055002 (2012)]. The WNL dynamics is found to be described by a 2D dissipative-dispersive nonlinear partial differential equation. The analytical and computational (for gas discharge plasma parameters) results predict strong viscosity induced Shilnikov homoclinic chaos, which, in turn, can cause a phase transition.

DOI: [10.1103/PhysRevE.103.023205](https://doi.org/10.1103/PhysRevE.103.023205)

## I. INTRODUCTION

The strongly coupled complex (dusty) plasma (SCCP) is a many-particle interacting dissipative system applicable in various fields of science and technology [1–4]. There are mainly two essential differences between the dissipative systems such as SCCP and the other various biological (or chemical) systems. These are the different interaction potentials and the presence of dissipation due to the collisions of particles with the atoms or molecules of the surrounding medium [1,4,5].

The dust particles interact with each other through a screened Coulomb potential of the Yukawa type,  $\Phi \sim Q^2 \exp(-\kappa)/(4\pi\epsilon_0\Delta)$ , where,  $Q$  is the dust charge,  $\epsilon_0$  is the permittivity,  $\Delta [= (3/4\pi n_d)^{1/3}]$ , where  $n_d$  is the dust density] is the mean interdust distance, and  $\kappa (= \Delta/\lambda_D)$ , where  $\lambda_D$  is the plasma Debye length) is the lattice parameter. This  $\Phi$  defines the coupling parameter  $\Gamma (= \Phi/T_d)$ , where  $T_d$  is the dust temperature in energy unit). The combined effect of interparticle interactions and ambient plasma lead to the formation of three-dimensional (3D) or quasi-2D strongly coupled ( $\Gamma \gg 1$ ) complex structures (fluids or crystals) in gas discharge plasma [3,6–10] that sustain three collective dust lattice modes [11–15]. In the presence of “plasma wake” [16–18], the coupling of two of these modes triggers mode coupling instability that causes crystal melting [19–23].

In dissipative strongly coupled systems, kinematic viscosity ( $\nu$ ) is one of the fundamental parameters that reflects the nature of the interparticle potentials and characterizes its thermodynamics [1,24,25], whereas the shear viscosity is effectively negligible [26,27]. The collisions between the dust particles and atoms or molecules of the surrounding neutral gas exert a strong influence on the viscous properties of dust particles [27–35]. It is observed that with increasing dust-neutral collision frequency ( $\nu_{dn}$ ),  $\nu$  decrease (increase) at low (high)  $\Gamma$  [27–30].

Experimental and theoretical results [13,36–52] confirm that in response to the relatively large amplitude disturbances (due to the intrinsic nonlinearities of interdust interactions), SCCP hosts a wealth of nonlinear collective structures. Interestingly, it sustains dissipative solitons for weak or moderate dust-neutral collision ( $\nu_{dn} \lesssim \omega^*$ , where

$\omega^* = [\partial_{rr}^2 \Phi|_{r=\Delta}/(2M)]^{1/2}$  is the characteristic dust-dust frequency and  $M$  is the constant dust mass) [36–40,45–47,57] and shock for weak or moderate viscosity ( $\nu \lesssim \omega^* \Delta^2$ ) [48,49,51,52]. However, the nonlinear transport processes in strongly dissipative ( $\nu^* = \nu/\omega^* \Delta^2 \gg 1$  and  $\nu_{dn}^* = \nu_{dn}/\omega^* \gg 1$ ) SCCP [27] are still an open question.

In this work, we present a theoretical and computational study of the weakly nonlinear (WNL) transport properties of a quasilongitudinal (QL) dust lattice wave (DLW) in recently observed highly viscous, strongly coupled, weakly ionized gas discharge plasmas where dust-neutral collisions have a strong influence on kinematic viscosity [27–29,32,33]. For the WNL dynamics, the SCCP is considered as the continuum medium under the assumption that  $\Delta$  is much less than the typical characteristic scale length ( $L$ ). A dissipative-dispersive (DD) nonlinear partial differential equation (NLPDE) is developed that governs the WNL dynamics of a QLDLW by employing the well-known reductive perturbation technique (RPT) [53]. This equation is solved analytically and numerically on the basis of gas discharge plasma parameters by posing the problem as a 3D autonomous nonlinear dynamical system. Depending on the strength of the viscosity, Mach number, direction of propagation, and wave number, the results predict (i) periodic and quasiperiodic nonlinear structures, (ii) Shilnikov homoclinic chaos, and (iii) the usual shock structure in highly dissipative SCCP.

The manuscript is organized in the following manner: The NLPDE is developed in Sec. II. The nonlinear analysis is described in Sec. III. The computational results with graphical representations are discussed in Sec. IV. Finally, a brief summary of the results and its possible applications are discussed in Sec. V.

## II. WEAKLY NONLINEAR DYNAMICS OF QUASILONGITUDINAL DUST LATTICE WAVE

The homogeneous plasma is composed of neutrals, electrons, ions, and nonemitted dust particles with large (constant) negative charge  $Q = -Ze$  ( $Z \sim 10^3$ – $10^5$  is the number of electrons that reside on the dust particles and  $e$  is the electron

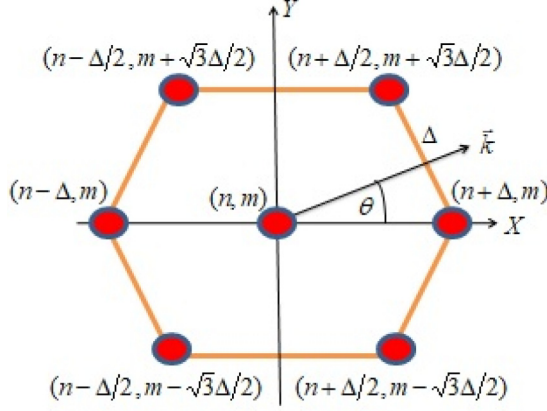


FIG. 1. Elementary monolayer 2D hexagonal lattice cell. Coordinate is  $(x_s = \Delta(n + m/2), y_s = m\sqrt{3}\Delta/2)$ ,  $s = (n, m) \in I = \{(0, \pm 1), (\pm 1, 0), (1, -1), (-1, 1)\}$ .

charge). Experimental observations [27–29,32,33] reveal that the physical properties of 2D SCCPs have two singular points: the first one relates to the liquid-to-hexatic phase transition at effective coupling parameter  $\Gamma^* = [\Gamma(\kappa^2 + 2\kappa + 2)/2] \approx 98 \pm 3$  and the second one at  $\Gamma^* \approx 154 \pm 4$  that corresponds to the crystallization with the hexagonal latex (hexatic-to-solid phase transitions). For the geometrical modeling of this crystalline structure, we use the “dust lattice string” model [13,38,41–43,46,50,54], allowing for the 2D motion, in the longitudinal (horizontal, along the  $X$  axis, with site ordering denoted by the index  $n$ ) and transverse (vertical, along the  $Y$  axis, with site locations denoted by  $m$ ) directions, as shown in Fig. 1.

The dust particles interact through the Debye-Hückel interaction potential (Yukawa potential) and the corresponding interdust force between  $s$ th and  $\acute{s}$ th ( $s, \acute{s} \in I$ ) particle is given by

$$\vec{F} = - \sum_{s \neq \acute{s}} \nabla_{r_s} \left[ \frac{Q^2}{4\pi\epsilon_0 r_{\acute{s},s}} \exp\left(-\frac{r_{\acute{s},s}}{\lambda_D}\right) \right]. \quad (1)$$

Here,  $r_{\acute{s},s} = |r_{\acute{s}} - r_s|$  and assume  $\vec{r}_{\acute{s},s} - \vec{r}_{\acute{s},s}(0) = d_L(\acute{s}, s)\hat{x} + d_T(\acute{s}, s)\hat{y}$  [ $d_{L(T)}(\acute{s}, s) = d_{L(T)}(\acute{s}) - d_{L(T)}(s)$ ] is the longitudinal (transverse) component of relative displacement of the  $s$ th lattice from equilibrium position  $\vec{r}_{\acute{s},s}(0)$  due to weak external force.

The waves in SCCP are the elastic deformation of the lattices of dust particles that frequently collide with the neutral atoms. The system is not in thermodynamic equilibrium at every instant mainly because of dust-neutral collisions and also the finite velocity of internal motion of the system. Thus the diffusive processes that tend to return the elastic body to thermodynamic equilibrium will take place and make the motion irreversible. This energy dissipative mechanism causes “viscosity” in a strongly correlated system [55] as observed in experiments and simulations [27–32,34,35]. The corresponding dissipative force can be expressed in discrete relation as [49,50,55]

$$\vec{\mathcal{F}}_{\acute{s},s}(\text{vis}) = Mv\partial_t \left[ \frac{d_L(\acute{s}, s)\hat{x} + d_T(\acute{s}, s)\hat{y}}{\Delta^2} \right]. \quad (2)$$

An approximated analytical form of (normalized  $v$ )  $v^* \equiv v^*(\Gamma^*, v_{dn}^*, D^*)$  is provided in Ref. [27] as

$$v^* \left( = \frac{v}{\omega^* \Delta^2} \right) \approx \frac{2\sqrt{\pi}D^*}{3\Gamma^*(1+v_{dn}^*)} + \frac{\sqrt{\Gamma^*(1+v_{dn}^*)}}{32\sqrt{\pi}D^*}, \quad (3)$$

where  $D^* = D(v_{dn} + \omega^*)M/T_d$  and  $D$  is the diffusion coefficient.

The lattice parameter  $\kappa$  is assumed to be large ( $\kappa \gg 1$ ) so that the dust particles in the 2D hexagonal crystal (Fig. 1) interact with their six nearest neighbors. The “plasma wake” [16–18] effect (which plays an important role for  $\kappa \lesssim 1$ ) and external force (which accounts for the parabolic confinement potential for a stable 2D crystal and/or initial laser excitation triggering the oscillations in experiments which has no direct influence on transport processes) are not considered here. Then, the  $X(Y)$  component of the equation of motion of the  $s$ th particle can be written as

$$M\partial_t^2 d_L = F_X + \mathcal{F}_X, \quad M\partial_t^2 d_T = F_Y + \mathcal{F}_Y, \quad (4)$$

where  $d_{L(T)} \equiv d_{L(T)}(\acute{s}, s)$ , and  $F_{X(Y)}$  and  $\mathcal{F}_{X(Y)}$  are the  $X(Y)$  component of the forces [Eqs. (1) and (2)], respectively. In the absence of dissipation ( $v = 0$ ), following the standard procedure [41–43,56], one can easily derive the discrete dispersion relations for DLWs.

In strongly dissipative SCCP experiments [27–29,32,33], it is observed that the macroparticles form a 2D-fluid-like structure with hexagonal symmetry (Fig. 1). Also, in these experiments, the footprint diameter of an  $\text{Ar}^+$  laser beam that excites the SCCP is  $\sim 3 \times 10^3 \mu\text{m}$  ( $= L$ ) and  $\Delta \sim (550 \pm 100) \mu\text{m}$  so that  $\Delta \ll L$ . These experimental conditions permit us to adopt the continuum approximation, which is very convenient to model a fluidlike medium. Since this approximation erases the molecular discontinuities by averaging the microscopic quantities, it converts the difference equations into differential equations for  $d_{L(T)}$  and neglects the nonlinear effects due to the particle discreteness [13,38,41–43,46,50,54]. Moreover, the equations under the continuum approximation well explain the experimentally observed nonlinear phenomena in SCCP [37–39,57].

In the continuum approximation,  $s = (n, m)$  is considered as a quasicontinuous variable [coordinate  $(x, y)$ ]. By expanding  $d_{L(T)}(\acute{s}, s)$  in the Taylor’s series up to the terms  $O(\Delta/L)^4$ , the viscous dissipative force [Eq. (2)] can be approximated as

$$\mathcal{F}_{X(Y)} \approx \left( \frac{3M}{2} \right) v\partial_t \left[ \nabla^2 \left( 1 + \frac{\Delta^2}{16} \nabla^2 \right) d_{L(T)} \right], \quad (5)$$

where  $\nabla^2 \equiv \partial_{xx}^2 + \partial_{yy}^2$ . For weak external harmonic disturbance of the form  $d_L, d_T \sim \exp i(\omega t - k_x x - k_y y)$ , where  $\omega$  ( $\omega \equiv \omega/\omega^*$ ) is the frequency,  $k_x = k \cos \theta$  ( $k_y = k \sin \theta$ ) ( $k \equiv k\Delta$ ) is the wave number along the  $X(Y)$  axis, and  $\theta$  is the angle of the wave vector  $\vec{k}$  ( $k = |\vec{k}|$ ) with the  $X$  axis (Fig. 1), the dissipative force (5) in  $(\omega, k)$  space becomes

$$\mathcal{F}_{X(Y)}(\omega, k) = -i\omega v^* k^2 \left( \frac{3M}{2} \right) \left( 1 - \frac{k^2}{16} \right) d_{L(T)}. \quad (6)$$

This clearly shows that in the sufficiently long wavelength ( $k \rightarrow 0$ ), the wave suffers the usual viscous damping. On the other hand, the wave suffers an instability for short wavelength perturbations ( $k > 4$ ). Such strong viscosity induced

instability is observed in fluid dynamics [58,59] and also in a 1D lattice chain falling in a viscous fluid [60].

However, here we are interested in studying the effects of strong viscosity ( $v^* \gg 1$ ) on the WNL dynamics of QLDLW by employing the well-known RPT [53]. Accordingly, we assume that the amplitude of the nonlinear wave is proportional to  $\epsilon$  ( $0 < \epsilon \lesssim 1$ ) [53] and introduce slow space ( $\xi, \zeta$ ) and time ( $\tau$ ) variables in terms of the small parameter  $\epsilon$  as [41,42,46]

$$\xi = \epsilon \Delta^{-1}(x - \omega^* \Delta t), \quad \zeta = \epsilon^2 \Delta^{-1}y, \quad \tau = \epsilon^3 \omega^* t. \quad (7)$$

For QL wave dynamics, the transverse displacement ( $d_T$ ) has a higher-order smallness than the amplitude of longitudinal displacement ( $d_L$ ) and thereby, for consistent perturbation  $d_{L(T)}$ , is represented as

$$d_L \sim \epsilon \tilde{d}_L \text{ and } d_T \sim \epsilon^2 \tilde{d}_T. \quad (8)$$

Experimental and numerical simulation results [27–29,32,33] around the second singular point ( $98 \leq \Gamma^* \leq 161$ , where crystallization with the hexagonal structure forms) estimate that  $v^* \sim O(10)$  [for a dust particle of radius  $a \approx 1 \mu\text{m}$ ,  $v_{dn}^* \sim O(10)$ , and  $\kappa \gtrsim 1.5$ ]. In particular,  $a = 0.95 \mu\text{m}$ ,  $\kappa = 2$ ,  $v_{dn}^* \approx 10$ , and  $\Gamma^* \approx 100$  estimate  $v^* \approx 10$  [27]. Thus to incorporate such strong viscosity in WNL transport, we consider the following scaling:

$$v^* = v_0 \epsilon^{-1}, \quad (9)$$

where  $v_0 = O(1)$  (of the order of unity). Note that if  $v^*$  is not so large, one can still use the same substitution, but now  $v_0$  should be small. This does not present any hurdle to the subsequent theoretical analysis [53].

Finally, by applying continuum approximation to Eqs. (1), (2), and (4), and then transforming the continuum equations in ( $\xi, \zeta, \tau$ ) variables [using scalings (7)–(9)], we obtain [keeping terms  $O(\epsilon^5)$ ] the following NLPDE for the WNL transport of QLDLW in highly dissipative SCCP:

$$\partial_\xi [(1 + \eta \partial_\xi) u_\tau - \alpha u u_\xi + \beta u_{\xi\xi\xi} - \gamma u_{\xi\xi\xi\xi}] + \frac{1}{2} u_{\zeta\zeta} = 0. \quad (10)$$

Here,  $u = \Delta^{-1} \partial_\xi \tilde{d}_L$ ,  $u_\tau \equiv \partial_\tau u$ ,

$$\alpha = \frac{9}{64} \left[ \frac{2\kappa^3 + 5(\kappa^2 + 2\kappa + 2)}{\kappa^2 + 2\kappa + 2} \right],$$

$$\beta = \frac{11}{256}, \quad \eta = \frac{3v_0}{4} = \frac{3\epsilon v^*}{4}, \quad \gamma = \frac{3v_0}{64} = \frac{3\epsilon v^*}{64}. \quad (11)$$

The strong kinematic viscosity is responsible for the both (lower- and higher-) order dissipative terms  $\eta$  and  $\gamma$ . The term  $\beta$  is the usual dispersion and the last term in Eq. (10) arises due to the anisotropy. In the absence of dissipation ( $v_0 = 0$ ), we recover the Kadomtsev-Petviashvili (KP) II equation [61] for the WNL dynamics of QLDLW [41] and further, in one dimension (1D), the Korteweg–de Vries equation [62] for the WNL dynamics of DLW [13,54]. Dissipation is inherent in almost every physical system and therefore the derived DD NLPDE (10) should be applicable to all physical systems where such equation arises. The solutions of Eq. (10) are interesting and applicable in different fields of physics and mathematics as demonstrated later.

### III. NONLINEAR ANALYSIS

The first two invariants of the derived DD NLPDE (10),

$$\partial_\tau J = 0 \text{ and } \partial_\tau \mathcal{E} = \iint [\eta u_\tau u_\xi + \gamma (u_{\xi\xi})^2] d\xi d\zeta, \quad (12)$$

reveal that the mass ( $J = \iint u d\xi d\zeta$ ) is conserved, but the energy ( $\mathcal{E} = \frac{1}{2} \iint u^2 d\xi d\zeta$ ) is not conserved so that Eq. (10) is non-Hamiltonian and not exactly integrable [63]. For  $v_0 = 0$ , Eq. (10) is believed to be stable for a plane-wave solution and possess a large family of interesting soliton solutions [63]. Thus, in the presence of weak dissipation ( $v_0 \neq 0$ ), one can employ the soliton perturbation technique [64] to find an approximated (leading-order) soliton solution [46] of the NLPDE (10).

However, here we are interested to find the other non-trivial solutions, which will help us to gain insight into the complexity of the dynamics (in the presence of higher-order dissipation). To achieve this goal, we follow Whitham [65] and analyze the NLPDE (10) in a stationary plane-wave frame,

$$\chi = \gamma^{-1/3} k_\xi^{-4/3} (V_f \tau - k_\xi \xi - k_\zeta \zeta).$$

The frame velocity  $V_f$  is related to Mach number ( $\mathcal{M}$ ) through the relation

$$\mathcal{M} = \frac{\omega^* \Delta + \epsilon^2 V_f}{\omega^* \Delta} = 1 + \epsilon^2 \left( \frac{V_f}{\omega^* \Delta} \right) \Rightarrow V_f \propto (\mathcal{M} - 1). \quad (13)$$

Interestingly, in the linear limit, we recover the usual relation  $\mathcal{M} = 1$ . In the  $\chi$  frame, by integrating Eq. (10) twice and choosing integration constants as zeros (Galilean symmetric group invariant), we construct the 3D autonomous nonlinear system,

$$\dot{\mathbf{X}} \equiv [\dot{\phi}, \dot{\psi}, \dot{\varphi}]^T = \left[ \psi, \varphi, \phi \left( U - \frac{\phi}{2} \right) - \varepsilon \psi - \delta \varphi \right]^T, \quad (14)$$

where  $\cdot \equiv d/d\chi$ ,  $\phi = -\alpha k_\xi u$ ,  $\dot{\phi} = \psi$ ,  $\dot{\psi} = \varphi$ , and

$$U = V_f - 0.5 k_\xi \tan^2 \theta, \quad \delta = 0.33 k_\xi^{1/3} v_0^{-2/3},$$

$$\varepsilon = 2.1 V_f k_\xi^{-5/3} v_0^{2/3}. \quad (15)$$

The system (14) is a dissipative system as  $\nabla \cdot \dot{\mathbf{X}} = -\delta < 0$  ( $\delta > 0$ ). The volume ( $\Upsilon$ ) satisfies the equation

$$\dot{\Upsilon} = \int_{\Upsilon} \nabla \cdot \dot{\mathbf{X}} d\Upsilon \Rightarrow \Upsilon(\chi) = \Upsilon(0) e^{-\delta \chi}.$$

This clearly shows that  $\Upsilon$  contracts as  $\chi$  advances, and thereby an arbitrary set of initial points in phase space ( $\phi, \psi, \varphi$ ) gradually condenses into a region of zero volume. The system (14) possesses two critical points, namely,

$$c_0 = (0, 0, 0) \text{ and } c_1 = (2U, 0, 0). \quad (16)$$

The nature of  $c_0(c_1)$  is determined by the eigenvalue ( $\lambda$ ) of the characteristic equation

$$\lambda^3 + \delta \lambda^2 + \varepsilon \lambda \mp U = 0. \quad (17)$$

However, for nonlinear analysis, we consider only the point  $c_0$  as it corresponds to the equilibrium state.

TABLE I. The values of  $\Gamma^*$ , nonlinear coefficient ( $\alpha$ ), and  $\nu^*$  for different  $\kappa$ . The values of  $\nu^*$  are calculated from formula (3). The value of the normalized diffusion coefficient  $D^* \simeq 0.1$  for  $130 \leq \Gamma^* \leq 160$  [28].

$\kappa$	$\Gamma^*$	$\alpha$	$\nu^*$
2	155	0.93	20.80
2.1	149	0.95	20.40
2.2	143	0.97	20.01
2.3	137	0.99	19.60
2.4	130	1.01	19.09

IV. NUMERICAL ANALYSIS

The numerical simulations are carried out for the typical gas discharge laboratory plasma parameters [27–29]: electron temperature ( $T_e$ ) = 3 eV, ion temperature ( $T_i$ ) = 0.03 eV, ion mass ( $m_i$ ) =  $6.69 \times 10^{-26}$  kg, and neutral density ( $n_n$ ) =  $8.4 \times 10^{21} \text{ m}^{-3}$  (pressure = 35 Pa). The dust (melamine formaldehyde) mass density =  $1.5 \times 10^3 \text{ kg m}^{-3}$ ,  $a = 0.95 \text{ }\mu\text{m}$  ( $M = 5.4 \times 10^{-15} \text{ kg}$ ),  $T_d = 0.03 \text{ eV}$ ,  $\Delta = 420 \text{ }\mu\text{m}$ , and  $\kappa = 2$ . These parameters estimate  $Q = -1.42 \times 10^3 e$ ,  $\omega^* \sim 20 \text{ rad s}^{-1}$ ,  $\nu_{dn} \sim 1.7 \times 10^2 \text{ rad s}^{-1}$  ( $\nu_{dn}^* \sim 8.5$ ), and  $\Gamma^* \sim 155$  [27–29]. This estimated value of  $\Gamma^*$  is large enough to predict a hexagonal latex structure [29]. Also, according to these experimental conditions,  $L \sim 3 \times 10^3 \text{ }\mu\text{m}$  so that  $\Delta/L \approx 0.14 \ll 1$  justifies the quasicontinuum approximation used to derive the NLPDE (10). The values of different physical parameters are provided in Table I. The values of  $\nu^*$  in Table I justify the assumption  $\nu^* \gg 1$  and the perturbation scaling (9). In the computation, the frame velocity  $V_f (> 0)$  is estimated as

$$V_f = [1 + 0.5 k_\xi \tan^2 \theta / (1 - 2.1 k_\xi^{-5/3} \nu_0^{2/3})],$$

i.e.,  $\mathcal{M} \propto [2 + 0.5 k_\xi \tan^2 \theta / (1 - 2.1 k_\xi^{-5/3} \nu_0^{2/3})].$

We simulate the nonlinear system (14) for  $\nu_0 = 0.1, 0.8$  and  $\theta = 10^0$ .

First, we consider a small disturbance around  $c_0$  and then solve the system (14) with initial conditions  $\phi = c_0 + 10^{-3}$ ,  $\psi = 10^{-5}$ , and  $\varphi = 10^{-5}$ . For the long wavelength disturbance with  $k_\xi = 0.25$ , the critical point  $c_0$  is a saddle point [node for  $\nu_0 = 0.1$  and focus for  $\nu_0 = 0.8$  according to the eigenvalues of the Eq. (17)] and the disturbance develops into shocklike structures as illustrated in Fig. 2. The curves in this figure show the transitions of  $\phi$  from zero value to a fixed value with the oscillatory [Fig. 2(a); for weak

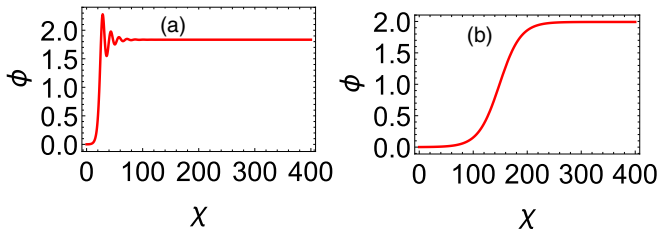


FIG. 2. Numerical solutions for  $k_\xi = 0.25$ . (a) Weak ( $\nu_0 = 0.1$ ) and (b) strong ( $\nu_0 = 0.8$ ) dissipations.

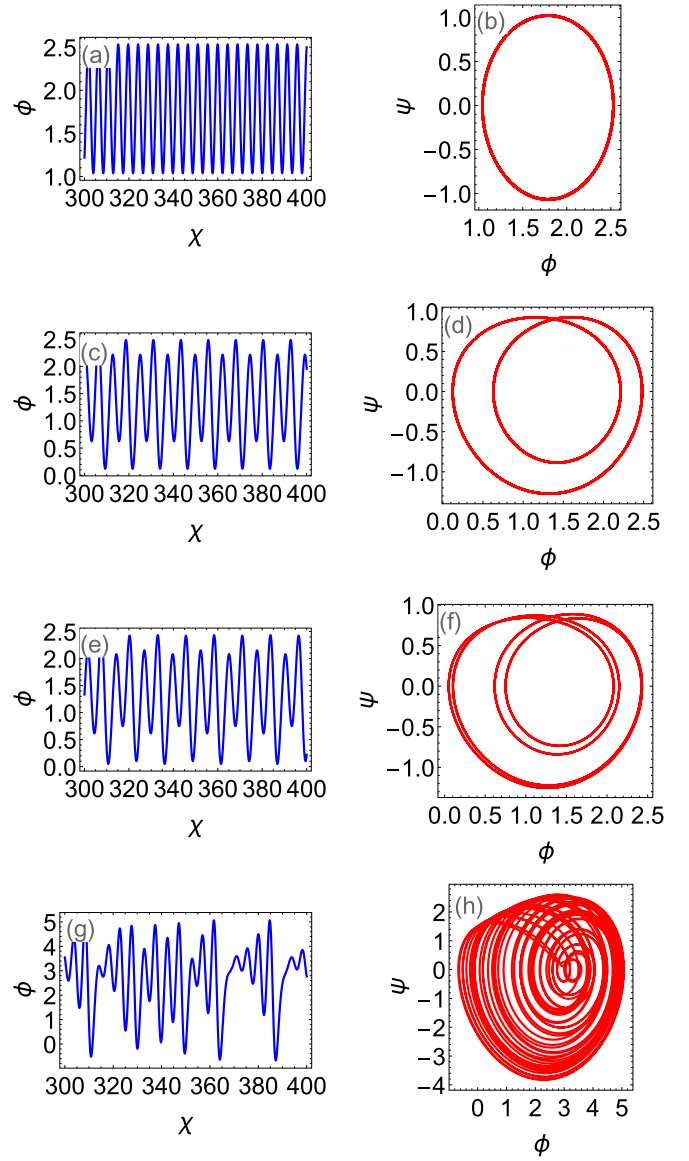


FIG. 3. Numerical solutions for short wavelength disturbances ( $k_\xi \gtrsim 1$ ) with strong dissipation  $\nu_0 = 0.8$ . Left and right panels are for  $\phi$  and projections of the corresponding phase-space diagrams. Bounded solutions are observed for  $0 \leq \chi \leq 10^4$ . Only solutions for subintervals of  $\chi$  are displayed for better clarity.

dissipation ( $\nu_0 = 0.1$ )] and monotonic [Fig. 2(b); for strong dissipation ( $\nu_0 = 0.8$ )] nature corresponding to the stable focus ( $c_1$ ) [66]. Viscous dissipation induced similar shock structures in weakly dissipative SCCP are observed in theory and experiment [48–51].

The physical system (14) is then simulated for relatively short wavelength disturbances ( $k_\xi \gtrsim 1$ ). A series of bifurcated states of (14) for a small disturbance around  $c_0$  is shown graphically in Fig. 3. This figure reveals that increasing  $k_\xi$  eventually forms a limit cycle [Figs. 3(a) and 3(b):  $k_\xi = 1$ ], then bifurcates to a period-doubling [Figs. 3(c) and 3(d):  $k_\xi = 1.33$ ; Figs. 3(e) and 3(f):  $k_\xi = 1.35$ ] and, finally, leads to a complex structure [Figs. 3(g) and 3(h):  $k_\xi = 1.5$ ]. The transitions of the qualitative behavior of  $\phi$  for different  $k_\xi$

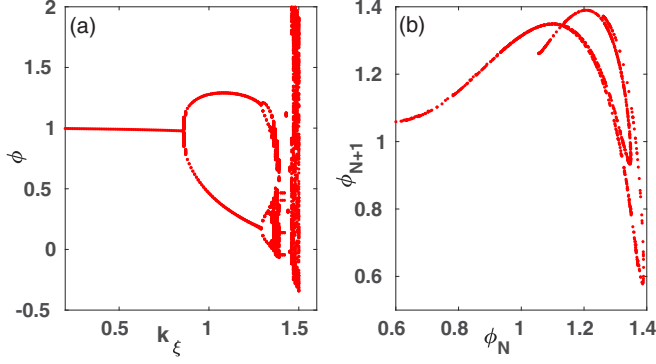


FIG. 4. (a) Bifurcation diagram of the system (14) with respect to  $k_\xi$  and (b) Poincaré return map of  $\phi$  for  $k_\xi = 1.5$ .

are shown in the bifurcation diagram in Fig. 4(a). This figure clearly shows that with the increase of  $k_\xi$ , the transitions occur through the formation of periodic (limit cycle)  $\rightarrow$  quasiperiodic (period-doubling)  $\rightarrow$  complex structure.

To analyze the qualitative behavior of the complex structure observed in Figs. 3(g) and 3(h) for  $k_\xi = 1.5$ , we construct the following 1D Poincaré return map [67–69] as

$$\phi_{N+1} = f(\phi_N).$$

This return map is constructed from the  $\chi$  series data of the variable  $\phi$  by collecting the local maxima of  $\phi$  in such a way that the  $(N + 1)$ th local maxima  $\phi_{N+1}$  of  $\phi$  is a function  $f$  of the  $N$ th local maxima  $\phi_N$ . The first return map for  $k_\xi = 1.5$  (constructed with the series of the maxima of  $\phi$ ) is plotted in Fig. 4(b). A close inspection of this figure clearly reveals that the points are densely populated with irregular distributions (without any known pattern). Such first-return map is the characteristic of chaotic oscillations [67–69].

Also the numerical solution of the characteristic equation (17) for the short wavelength perturbations ( $k_\xi \gtrsim 1$ ) around  $c_0$  reveals that the eigenvalues (say,  $\lambda_1$ ,  $\lambda_2$ , and  $\lambda_3$ ) of the nonlinear system (14) are of the form

$$\lambda_1 = \Lambda > 0 \text{ and } \lambda_{2,3} = -\rho \pm i\Omega \text{ } (\rho > 0).$$

This implies that  $c_0$  is a saddle focus. Thus for the analytical characterization of the computational results described in Fig. 3 (for the short wavelength perturbations), we follow the mathematical recipes of Refs. [70,71]. Accordingly, we define the saddle index ( $\mu$ ) and the first (second) saddle value ( $\sigma_{1(2)}$ ) as

$$\mu = \frac{|\text{Re } \lambda_{2,3}|}{|\lambda_1|} = \frac{\rho}{\Lambda}, \quad \sigma_{1(2)} = \lambda_1 + 1(2)\text{Re } \lambda_{2,3}. \quad (18)$$

The values of  $\mu$  and  $\sigma_{1(2)}$  of the solutions in Fig. 3 are shown in Table II. The integral curves of the linearized system of (14) can be written as  $\phi \simeq \phi_{1D} + \phi_{2D}$ , where

$$\phi_{1D} = Ae^{\Lambda\chi} \text{ and } \phi_{2D} = Be^{-\rho\chi} \cos(\Omega\chi + \phi_0)$$

( $A$ ,  $B$ , and  $\phi_0$  are constants), and satisfy biasymptotic conditions,

$$\phi \simeq \phi_{1D}|_{\chi \rightarrow -\infty} \text{ and } \phi \simeq \phi_{2D}|_{\chi \rightarrow \infty}.$$

TABLE II. Values of  $\mu$  and  $\sigma_{1(2)}$  for different curves in Fig. 3. For fixed values of  $\theta$  and  $v_0$ ,  $\mu = \mu(k_\xi)$ .

Fig. 3	$k_\xi$	$\mu$	$\sigma_1$	$\sigma_2$
(a),(b)	1	1.02	$-4.6 \times 10^{-3}$	-0.41
(c),(d)	1.33	0.93	$4 \times 10^{-2}$	-0.44
(e),(f)	1.35	0.92	$4.2 \times 10^{-2}$	-0.46
(g),(h)	1.5	0.84	0.1	-0.50

Thus, starting from  $c_0$  at  $\chi = -\infty$ , all the integral curves of the field flow escape from the vicinity of it, but spirally return back at  $\chi = \infty$ . These two integrals correspond to two invariant manifolds intersecting in a neighborhood of  $c_0$ : a 1D unstable manifold  $M_{1D}^u(c_0)$  and a 2D stable manifold  $M_{2D}^s(c_0)$ . The intersection of these two manifolds [ $M_{1D}^u(c_0) \approx M_{2D}^s(c_0)$ ] forms a homoclinic loop [70], as illustrated in Fig. 5 for  $k_\xi = 1.51$ .

The nonlinear system (14) with the homoclinic loop of  $c_0$  (saddle focus) forms a bifurcation manifold  $\mathcal{B}^1$  of codimension 1 in the Banach space of the system with a smooth topology [70]. Hence, a small smooth perturbation around  $c_0$  of the vector field breaks the homoclinic loop. Later, for  $\mu > 1$  ( $\sigma_{1(2)} < 0$ ), the transition over  $\mathcal{B}^1$  leads to the emergence of a single, stable periodic orbit from the homoclinic loop [71] by forming a limit cycle, as observed in Figs. 3(a) and 3(b).

The computational results in Table II clearly show that for a fixed value of  $\theta$  and  $v_0$ ,  $\mu \propto k_\xi^{-1}$ , i.e., with the increase of  $k_\xi$ ,  $\mu$  decreases ( $\mu = 1$  is the boundary of the bifurcations) and a small disturbance triggers the system to the homoclinic explosion ( $\mu < 1$ ) by forming period-doubling structures [70,71], as illustrated in Figs. 3(c) and 3(d) and Figs. 3(e) and 3(f). All of these are clearly shown graphically in the bifurcation diagram in Fig. 4(a).

The first (second) saddle value  $\sigma_{1(2)}$  is the most positive (negative) at  $k_\xi = 1.5$  (shown in Table II) and the system is

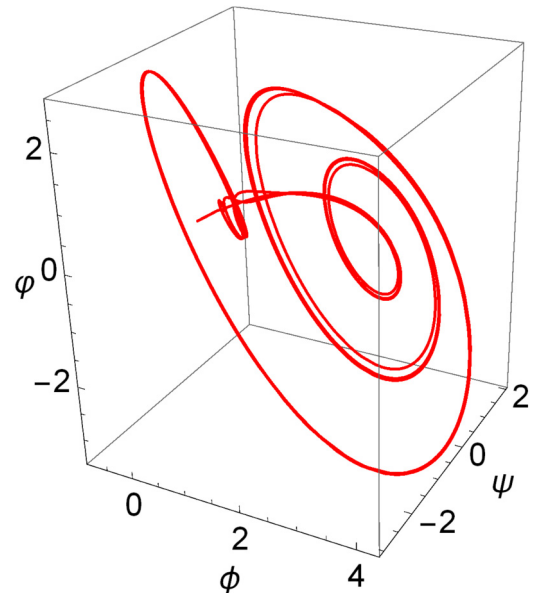


FIG. 5. Homoclinic loop around  $c_0$  for  $k_\xi = 1.51$ .

then very close to the homoclinic loop, as illustrated in Fig. 5 at  $k_\xi = 1.51$ . According to Shilnikov [70], the system (14) then possesses uncountably many nonperiodic trajectories (chaotic invariant sets). Thus, the complex structures (solutions) presented in Figs. 3(g) and 3(h), indeed, resemble the situation of a homoclinic chaos.

## V. DISCUSSIONS

In the quasicontinuum limit, a realistic DD nonlinear model [Eq. (10)] is developed to study the WNL transport of QLDLW in an experimentally observed highly dissipative SCCP [27–29]. The plane-wave nonlinear analysis of the derived DD NLPDE (10) and also the computational results reveal that for the long wavelength perturbations, the WNL wave possesses the usual shock solution. However, for the short wavelength perturbations ( $k_\xi \gtrsim 1$ ), the WNL wave possesses a wide class of nonlinear structures such as periodic, quasiperiodic, and Shilnikov homoclinic chaotic structures.

Physically, an increase in wave number ( $k_\xi$ ) enhances and creates new perturbations in the collective dynamics that generates new harmonics. These harmonics interact among themselves (many wave interactions) and form coherence structures, which for suitable physical parameters show

chaotic dynamics [72]. This chaotic flow gives rise to energy diffusion (direct microscopic exchange of kinetic energy between structure and plasma) leading to an increase of particle kinetic energy, which, in turn, can cause a phase transition. Theoretically and experimentally, it is observed [19–23] that resonance instability due to mode coupling is responsible for the crystal melting. However, the result of this investigation reveals that strong viscosity induced homoclinic chaos could also be a viable physical process for crystal melting. This is theoretical evidence of the existence of a phase transition through homoclinic chaos due to strong viscous effects.

Finally, the computational results are on the basis of real dissipative SCCP experiments, so we expect that the results of this work could be observed in future experiments.

## ACKNOWLEDGMENTS

The author thanks the three referees for their careful reading and offering of constructive suggestions to improve the manuscript. The author also thanks Dr. S. Poria, Department of Applied Mathematics, University of Calcutta, for his stimulating influence on the numerical simulation during the course of this work.

- 
- [1] V. E. Fortov, A. V. Ivlev, S. A. Khrapak, A. G. Khrapak, and G. E. Morfill, *Phys. Rep.* **421**, 1 (2005).
  - [2] S. Vladimirov, K. Ostrikov, and A. Samarian, *Physics and Applications of Complex Plasmas* (Imperial College, London, 2005).
  - [3] H. M. Thomas and G. E. Morfill, *Nature (London)* **379**, 806 (1996).
  - [4] G. E. Morfill and A. V. Ivlev, *Rev. Mod. Phys.* **81**, 1353 (2009).
  - [5] S. Hamaguchi, R. T. Farouki, and D. H. E. Dubin, *Phys. Rev. E* **56**, 4671 (1997).
  - [6] J. H. Chu and Lin I, *Phys. Rev. Lett.* **72**, 4009 (1994).
  - [7] H. M. Thomas, G. E. Morfill, V. Demmel, J. Goree, B. Feuerbacher, and D. Möhlmann, *Phys. Rev. Lett.* **73**, 652 (1994).
  - [8] A. Melzer, T. Trottenberg, and A. Piel, *Phys. Lett. A* **191**, 301 (1994).
  - [9] G. A. Hebner, M. E. Riley, and K. E. Greenberg, *Phys. Rev. E* **66**, 046407 (2002).
  - [10] J. B. Pieper, J. Goree, and R. A. Quinn, *Phys. Rev. E* **54**, 5636 (1996).
  - [11] S. Nunomura, J. Goree, S. Hu, X. Wang, and A. Bhattacharjee, *Phys. Rev. E* **65**, 066402 (2002).
  - [12] S. Nunomura, J. Goree, S. Hu, X. Wang, A. Bhattacharjee, and K. Avinash, *Phys. Rev. Lett.* **89**, 035001 (2002).
  - [13] F. Melandso, *Phys. Plasmas* **3**, 3890 (1996).
  - [14] P. K. Kaw and A. Sen, *Phys. Plasmas* **5**, 3552 (1998).
  - [15] J. K. Meyer, I. Laut, S. K. Zhdanov, V. Nosenko, and H. M. Thomas, *Phys. Rev. Lett.* **119**, 255001 (2017).
  - [16] S. V. Vladimirov and M. Nambu, *Phys. Rev. E* **52**, R2172 (1995).
  - [17] S. V. Vladimirov and O. Ishihara, *Phys. Plasmas* **3**, 444 (1996).
  - [18] A. Melzer, V. A. Schweigert, and A. Piel, *Phys. Rev. Lett.* **83**, 3194 (1999).
  - [19] A. V. Ivlev and G. Morfill, *Phys. Rev. E* **63**, 016409 (2000).
  - [20] S. K. Zhdanov, A. V. Ivlev, and G. E. Morfill, *Phys. Plasmas* **16**, 083706 (2009).
  - [21] L. Couëdel, V. Nosenko, A. V. Ivlev, S. K. Zhdanov, H. M. Thomas, and G. E. Morfill, *Phys. Rev. Lett.* **104**, 195001 (2010).
  - [22] B. Liu, J. Goree, and Y. Feng, *Phys. Rev. Lett.* **105**, 085004 (2010).
  - [23] K. Qiao, J. Kong, E. V. Oeveren, L. S. Matthews, and T. W. Hyde, *Phys. Rev. E* **88**, 043103 (2013).
  - [24] V. Nosenko and J. Goree, *Phys. Rev. Lett.* **93**, 155004 (2004).
  - [25] B. Liu and J. Goree, *Phys. Rev. Lett.* **94**, 185002 (2005).
  - [26] C. V. Johnson and P. Steinberg, *Phys. Today* **63**(5), 29 (2010).
  - [27] V. E. Fortov, O. F. Petrov, O. S. Vaulina, and R. A. Timirkhanov, *Phys. Rev. Lett.* **109**, 055002 (2012).
  - [28] O. S. Vaulina and I. E. Dranzhevski, *Phys. Scr.* **73**, 577 (2006).
  - [29] T. S. Ramazanov and K. N. Dzhumagulova, *Contrib. Plasma Phys.* **48**, 357 (2008).
  - [30] Z. Donko, J. Goree, and P. Hartmann, *Phys. Rev. E* **81**, 056404 (2010).
  - [31] Y. Feng, J. Goree, and Bin Liu, *Phys. Rev. Lett.* **105**, 025002 (2010).
  - [32] A. V. Gavrikov, D. N. Goranskaya, A. S. Ivanov, O. F. Petrov, R. A. Timirkhanov, N. A. Vorona, and V. E. Fortov, *J. Plasma Phys.* **76**, 579 (2010).
  - [33] O. S. Vaulina, I. E. Drangevski, X. G. Adamovich, O. F. Petrov, and V. E. Fortov, *Phys. Rev. Lett.* **97**, 195001 (2006).
  - [34] Y. Feng, J. Goree, and B. Liu, *Phys. Plasmas* **18**, 057301 (2011).
  - [35] P. Hartmann, M. C. Sandor, A. Kovacs, and Z. Donko, *Phys. Rev. E* **84**, 016404 (2011).
  - [36] S. V. Vladimirov, P. V. Shevchenko, and N. F. Cramer, *Phys. Rev. E* **56**, R74 (1997).

- [37] D. Samsonov, A. V. Ivlev, R. A. Quinn, G. Morfill, and S. Zhdanov, *Phys. Rev. Lett.* **88**, 095004 (2002).
- [38] S. K. Zhdanov, D. Samsonov, and G. E. Morfill, *Phys. Rev. E* **66**, 026411 (2002).
- [39] S. Nunomura, S. Zhdanov, G. E. Morfill, and J. Goree, *Phys. Rev. E* **68**, 026407 (2003).
- [40] R. Heidemann, S. Zhdanov, R. Sütterlin, H. M. Thomas, and G. E. Morfill, *Phys. Rev. Lett.* **102**, 135002 (2009).
- [41] W. Duan, G. Wan, X. Wang, and M. Lin, *Phys. Plasmas* **11**, 4408 (2004).
- [42] W. Duan, J. Parkes, and M. Lin, *Phys. Plasmas* **12**, 022106 (2005).
- [43] B. Farokhi, I. Kourakis, and P. K. Shukla, *Phys. Plasmas* **13**, 122304 (2006).
- [44] V. Koukoulouyannis and I. Kourakis, *Phys. Rev. E* **80**, 026402 (2009).
- [45] S. Ghosh, M. R. Gupta, N. Chakrabarti, and M. Chaudhuri, *Phys. Rev. E* **83**, 066406 (2011).
- [46] S. Ghosh, *Phys. Rev. E* **90**, 033108 (2014).
- [47] S. K. Sharma, A. Boruah, and H. Bailung, *Phys. Rev. E* **89**, 013110 (2014).
- [48] D. Samsonov, S. K. Zhdanov, R. A. Quinn, S. I. Popel, and G. E. Morfill, *Phys. Rev. Lett.* **92**, 255004 (2004).
- [49] S. Ghosh, *JETP Lett.* **87**, 281 (2008); **88**, 702 (2008); *Contrib. Plasma Phys.* **48**, 569 (2008).
- [50] S. Ghosh, *Phys. Plasmas* **16**, 103701 (2009).
- [51] S. Jaiswal, P. Bandyopadhyay, and A. Sen, *Phys. Plasmas* **23**, 083701 (2016).
- [52] A. Kananovich and J. Goree, *Phys. Rev. E* **101**, 043211 (2020).
- [53] T. Tanuiti, *Suppl. Prog. Theor. Phys.* **55**, 1 (1974).
- [54] I. Kourakis and P. K. Shukla, *Eur. Phys. J. D* **29**, 247 (2004).
- [55] L. D. Landau and E. M. Lifshitz, *Theory of Elasticity* (Pergamon Press, London, 1959), p. 122.
- [56] B. Farokhi, I. Kourakis, and P. K. Shukla, *Phys. Lett. A* **355**, 122 (2006).
- [57] K. Avinash, P. Zhu, V. Nosenko, and J. Goree, *Phys. Rev. E* **68**, 046402 (2003).
- [58] D. J. Benny, *J. Math. Phys.* **45**, 150 (1966).
- [59] T. B. Benjamin, *J. Fluid Mech.* **2**, 554 (1957).
- [60] J. M. Crowley, *J. Fluid Mech.* **45**, 151 (1971).
- [61] B. B. Kadomtsev and V. I. Petviashvili, *Sov. Phys. Dokl.* **15**, 539 (1970).
- [62] D. Korteweg and G. de Vries, *Philos. Mag.* **39**, 422 (1895).
- [63] V. Yu. Belashov and S. V. Vladimirov, *Solitary Waves in Dispersive Complex Media* (Springer-Verlag, Berlin, 2005), p. 140.
- [64] V. I. Karpman and E. M. Maslov, *Sov. Phys. JETP* **46**, 281 (1977).
- [65] G. B. Whitham, *Linear and Nonlinear Waves* (Wiley-Interscience, New York, 1974).
- [66] R. S. Johnson, *J. Fluid Mech.* **42**, 49 (1970).
- [67] E. N. Lorenz, *J. Atmos. Sci.* **20**, 132 (1963).
- [68] D. Molenaar, H. J. H. Clercx, and G. J. F. van Heijst, *Phys. Rev. Lett.* **95**, 104503 (2005).
- [69] N. H. Packard, J. P. Crutchfield, J. D. Farmer, and R. S. Shaw, *Phys. Rev. Lett.* **45**, 712 (1980).
- [70] L. P. Shilnikov, *Soc. Math. Dokl.* **6**, 163 (1965); *Math. USSR Sbornik* **10**, 91 (1970).
- [71] L. A. Belyakov, *Math. Zametki* **36**, 838 (1974).
- [72] L. Sirovich, *Physica D* **37**, 126 (1989).